Tissue Imaging

DOI: 10.1002/ange.201104530

Simultaneous Photographing of Oxygen and pH In Vivo Using Sensor Films**

*Robert J. Meier, Stephan Schreml, Xu-dong Wang, Michael Landthaler, Philipp Babilas, and Otto S. Wolfbeis**

Optical imaging of chemical analytes such as CO_2,[1] H_2O_2,[2] oxygen,[3] Ca^{2+},[4] or pH[5] in vivo is a fast-growing field because these species can be observed and quantified over whole areas rather than at a single point of measurement. This feature is particularly important in biomedical sciences where large variations of such parameters can be found in even small areas (such as cells), and where sampling usually is impossible or would alter the actual concentration of the analyte (for example in the case of O_2). The distribution of such species is most often visualized using luminescence-based readout techniques,[6] and these can be based on measurement of intensity,[7] fluorescence lifetime (FLIM),[1,8] or of signals at two wavelengths (ratiometry),[9] for example. Referencing is mandatory to enable quantitative imaging and to eliminate effects caused by variations in the concentration and distribution of fluorescent probes. (For an introduction into methods for referencing, see the Supporting Information, Note 1.)

Herein we introduce the first method for simultaneous imaging of two parameters with only one image acquired by a conventional digital camera. An LED array placed in front of the camera is used for photoexcitation. The camera here also acts as a rudimental spectrometer for ratiometric imaging with one excitation wavelength and multiple (three-wavelength) readout. A sensor film with immobilized indicator probes is employed rather than dissolved probes which have limitations in terms of even dye distribution and toxicity. The detection scheme exploits the fact that data can be stored in the memory of a camera in three color channels (red/green/blue). This is used to separate the optical signals[10] for two parameters (pH, pO_2), but may also be applied to other kinds of dual sensing if appropriate materials are made available.

Practically all digital cameras make use of metal oxide semiconductor chips with red, green, and blue (RGB) "channels". These display distinct spectral sensitivities in the visible part of the spectrum (Supporting Information, Figure S1). Thus, a complete color picture is composed of three virtually independent data sets. Digital cameras are cheap, have a large dynamic range (14-bit in the RAW mode), can be quite small, and offer easy handling compared to other setups, such as CCD cameras and respective imagers. We show herein that the use of such photographic systems combined with the appropriate sensor films (also presented herein) allows for continuous imaging (and even recording of videos) of two different parameters simultaneously. The novel technique was applied in vivo to image oxygen and pH in acute and chronic cutaneous wounds of humans, because oxygen and pH particularly affect wound healing (Supporting Information, Note 2).[11]

Three dyes with emission peaks matching the three color channels of the camera (see spectra in the Supporting Information, Figure S1) were chosen from a multitude of conceivable candidates[12] to create a sensor film that can be read out by the RGB technique. Oxygen is detected by using the probe platinum(II)-5,10,15,20-tetrakis-(2,3,4,5,6-pentafluorophenyl)porphyrin (Pt-TPFPP (with its emission maximum at 650 nm; stored in the red channel). Fluorescein isothiocyanate (FITC; λ_{em} 530 nm; signal stored in the green channel) was used to sense pH. The signals of the two indicators were related to the intensity of the reference fluorophore diphenylanthracene (DPA; λ_{em} 440 nm; stored in the blue channel). All of the dyes were first incorporated into polymer microparticles and then placed in a biocompatible polymer film as shown below. The probes contained in the sensor film can be photoexcited with the 405 nm (purple) LEDs mounted in the form of a ring, in front of the camera (Supporting Information, Figure S2). The luminescence of the sensor (Figure 1 a) is recorded with a digital camera (Supporting Information, Figure S2) that is also equipped with a 435 nm long-pass optical filter to separate scattered blue excitation light from the recorded image.

To visualize the spatial distribution of pH and pO_2, a real-color RGB image of the sensor is recorded (Figure 1 b) and then split into the RGB color channels (Figure 1 c). The red luminescence of Pt-TPFPP decreases with increasing pO_2,

[*] Dr. R. J. Meier,[+] Dr. X. D. Wang, Prof. O. S. Wolfbeis
Institut für Analytische Chemie, Chemo- und Biosensorik
Universität Regensburg, 93040 Regensburg (Germany)
E-mail: otto.wolfbeis@chemie.uni-r.de
Homepage: http://www.wolfbeis.de
Dr. S. Schreml,[+] Prof. M. Landthaler, Dr. P. Babilas
Klinik und Poliklinik für Dermatologie
Universitätsklinikum Regensburg (Germany)
[+] These authors contributed equally to this work.

[**] The authors are grateful to the Deutsche Forschungsgemeinschaft for grants WO 669/9-1 and BA 3410/4-1, and the Novartis Foundation Novartis Graduate Scholarship (to S.S.). X.W. thanks the German Academic Exchange Service (DAAD) for a grant. The authors thank Josef Schroeder and Heiko Siegmund (Institute of Pathology) for electron microscopic images, Tim Maisch, Johannes Regensburger, and Francesco Santarelli (Department of Dermatology) for keratinocyte cultures and singlet oxygen detection, Karla Lehle and Christina Leykauf (Department of Cardiothoracic Surgery) for cell cultures and cytotoxicity tests, Judith Stolwijk (Institute of Analytical Chemistry, Chemo- and Biosensors) for confocal microscopic imaging, and Timo Lauber and Dietmar Schreml for their help with video processing.

Supporting information for this article is available on the WWW under http://dx.doi.org/10.1002/anie.201104530.

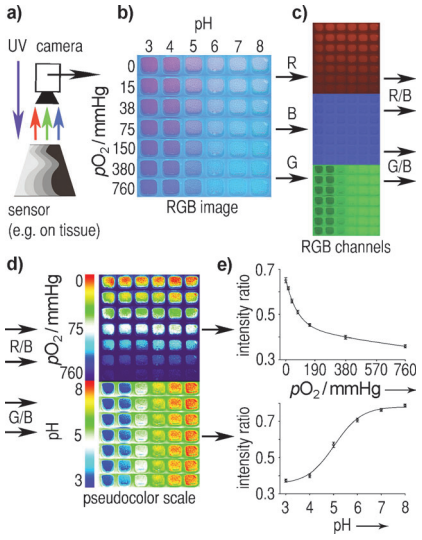

Figure 1. Sensing process and calibration plots. a) The sensor film is illuminated with UV light. The three dyes in the sensor layer emit red (R), green (G), and blue (B) light that is collected by a CMOS photodetector and stored in the memory of the camera. b) Real-color picture (RGB image) of a sensor array with different pH values and oxygen concentrations. c) The respective image is split into three independent color channel pictures. d) The ratio of red to blue channel pictures (R/B; displayed in pseudo colors) represents the oxygen response and shows the lack of cross-reactivity to pH. The ratio of green to blue channel pictures (G/B; also displayed in pseudo colors) reflects the response to pH and also demonstrates the lack of cross-reactivity to oxygen. e) Respective calibration plots for oxygen (bi-exponential decay fit) and pH (sigmoidal fit).

while the green luminescence of FITC increases with pH. The blue reference signal, in contrast, remains unaffected by both oxygen and pH (Supporting Information, Figure S3) as it is incorporated in a virtually impermeable polymer. The three signals can then be referenced by dividing the intensity values of each pixel of the respective picture (red or green channel) by the intensity values of "blue" pixels in the reference channel. Thus, the R/B ratio of each pixel represents the referenced response to oxygen (Figure 1 d). Calibration plots for oxygen (up to 760 mmHg; equivalent to 1013 hPa) follow a four-parameter bi-exponential decay fit (Figure 1 e). Oxygen partial pressure in the physiological range can be calculated by solving a mono-exponential fit for pO_2 (Supporting Information, Figure S4a) by using Equation (1):

$$pO_2[\mathrm{mmHg}] = -\frac{\ln\left(\frac{R/B-y_0}{a}\right)}{b} \qquad (1)$$

The calibration for pH (based on the ratio G/B; Figure 1 d) follows a sigmoidal fit. pH values between 3 and 8 can be calculated (Supporting Information, Figure S4b) by using Equation (2):

$$\mathrm{pH} = x_0 - \ln\left(\frac{y_0 + a - G/B}{G/B - y_0}\right) b \qquad (2)$$

Optical sensors can be affected by adverse effects of sample matrices if the indicator dyes are brought into direct contact with the biological sample. In case of sensors for in vivo use, the potential toxicity of indicators is another issue. Dyes were therefore either covalently bound to or incorporated into inert polymer microparticles (see the Experimental Section). The resulting particles were then incorporated in a biocompatible hydrogel to prevent particle leakage (Supporting Information, Figure S5). Microparticles were synthesized in sizes between 0.5 and 8 μm to exclude possible uptake by tissue. The use of microparticles has the additional advantage of preventing fluorescence resonance energy transfer (FRET) between the dyes[6] because the average distance of the dyes is much more than 10 nm, the maximal FRET distance. Conceivably, sensor nanoparticles may be used as well, but this implies the risk of leakage and cellular uptake.

Pt-TPFPP was incorporated into polystyrene particles (Pt-PS, 1–3 μm; Figure 2 a), and DPA into polyacrylonitrile particles (DPA-PAN, 0.5–1 μm; Figure 2 c). Both dyes are retained owing to hydrophobic interactions and their insolubility in water. FITC was covalently attached to aminocellulose particles (FITC-AC, 2–8 μm; Figure 2 b).[5] As a result, dyes do not leach out of the particles (Supporting Information, Figure S6). PS was chosen as the material of choice for the oxygen-sensitive particles owing to its excellent gas permeability and hydrophobicity, which renders it permeable to oxygen but not to water and protons. PAN, in contrast, is virtually impermeable to oxygen. AC is hydrophilic and rapidly penetrated by protons. The pK_a of fluorescein shifts from 6.8 to 5 upon conjugation to AC. This is beneficial in terms of sensing pH in tissue.[5] Residual

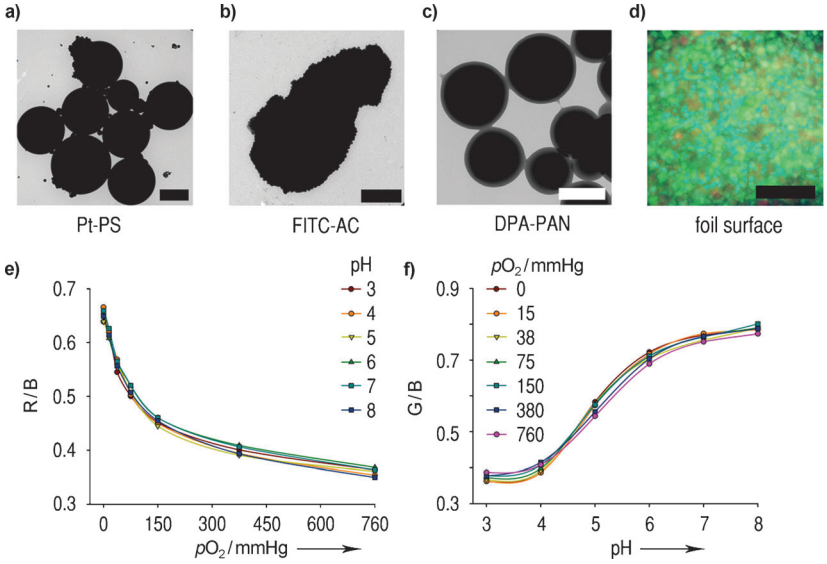

Figure 2. Characterization of the sensor. a–c) Transmission electron microscopy (TEM) images of a) Pt-PS (scale bar 2 μm); b) FITC-AC (scale bar 2 μm); and c) DPA-PAN (scale bar 0.5 μm). d) Fluorescence microscopy image of a poly(vinylidene chloride) (PVdC) foil coated with the sensor particles in a polyurethane hydrogel matrix. Neither e) oxygen (R/B) nor f) pH signals (G/B) showed cross-sensitivity for the other parameter.

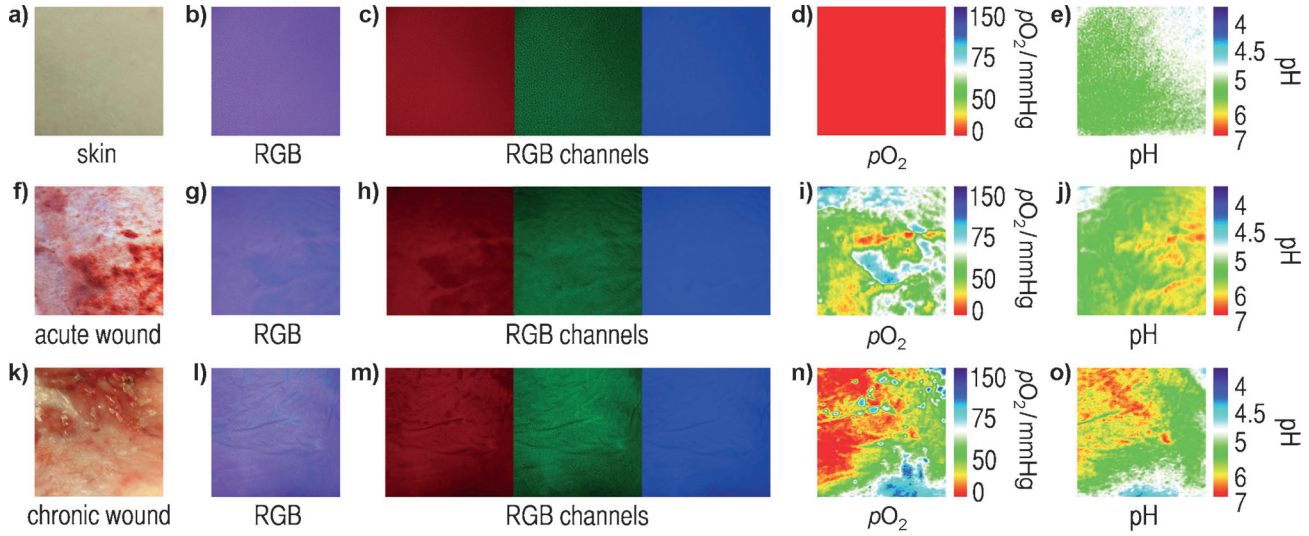

Figure 3. In vivo application of the dual sensor on the plain skin surface of a volar forearm (a–e), a skin graft donor site (postoperative, day 5) as a model for acute wound healing (f–j), and a chronic wound (k–o). a), f), and k) are pictures of skin and wound surfaces; b), g), and l) are the RGB pictures of skin and wound with an overlaying sensor. The picture is split into the three respective color channels (c, h, m). The R/B ratios in d), i), and n) show the distribution of oxygen; the G/B ratios show the pH distribution on the surface of skin and wound (e, j, o). For scaling, see the calibration plots in Figure 1 and the Supporting Information, Figure S4.

amino groups of AC were blocked with acetic anhydride to remove excess charges that may act as local buffer and slow down sensor response.

Sensor films (Supporting Information, Figure S7) for in vivo applications were created as described in the Supporting Information, Note 3. Potential cytotoxicity (Supporting Information, Figure S8) and cellular uptake (Supporting Information, Figure S9) was excluded prior to use on live human subjects (Supporting Information, Note 4). The potentially harmful generation of singlet oxygen was also investigated, as described in the Supporting Information, Note 5 and Figure S10, and photobleaching was excluded of playing a major role either (see the data in the Supporting Information, Note 6 and Figure S11). The response time to oxygen is 9 s, and to pH is 25 s. Both are short enough to enable real-time monitoring (Supporting Information, Note 7 and Figure S12). All measurements were started 1 min after the sensor was applied to the sample (buffers or wounds). The referenced signals for oxygen and for pH are neither cross-sensitive (Figure 2 e,f) nor significantly dependent on temperature (20–40 °C; Supporting Information, Figure S13).

The method was applied to simultaneously visualize oxygen and pH on tissue (Supporting Information, Note 8). Imaging of intact skin showed a virtually homogeneous distribution of oxygen and pH (Figure 3 a–e). The epidermis prevents diffusion of oxygen through skin, thus very low pO_2 are found on the surface of skin. The results confirm earlier experiments[8] obtained by luminescence lifetime imaging of pO_2 only. The pH values of the surface of the skin were found to range from 4.5 to 5.5.

To demonstrate the potential for 2D imaging, a heterogeneous chronic wound was visualized (Figures 3 k–o). Oxygen and pH values are indicative of a sustained inflammatory phase, especially the high pH values in the upper left part of Figure 3 o. This area is quite hypoxic, which is probably due to the high oxygen demand during inflammation and tissue formation during wound healing.

In summary, the RGB method for dual sensing[13] presented herein follows the trend for small and inexpensive analytical devices[14] and holds great promise for a remarkable simplification of multiple luminescence imaging compared to methods based on individual sensor spots.[15] It is paralleled by related work on dual sensing of alkali ions.[16] We believe that this sensor can further the understanding of the role of oxygen and local pH in biomedical sciences, for example, in wound healing, tumor metabolism, medical treatment efficacy, or tissue transplantation. The technique also paves the way for various other approaches towards multiple analyte sensing with different detection ranges or analyte combinations. Modified camera firmware with integrated mathematical processing even allows for recording movies and real-time simultaneous viewing of 2D distributions of two chemical parameters. Conceivably, the method can be extended to imaging temperature,[17] which is important to know in all kinds of chemical sensors and biosensors because all sensors are affected by temperature, and its effects have to be corrected for. We also believe that this referenced RGB method for dual imaging paves the way for numerous other sensing and imaging applications based on sensor paints[18] in areas such as medicine, environmental sciences, industrial (chemical) processes,[19] food technology,[20] biotechnology,[21] marine sciences,[22] and the automotive and aerospace industry,[17b,23] provided that respective sensor films are made available.

Experimental Section

Pt-PS microparticles were prepared using a polymerization method[24] by dissolving α,α′-azoisobutyronitrile (62.5 mg) in a mixture of styrene (7.0 mL) and methacrylic acid (60 μL) and mixing the

solution with ethanol (25 mL) containing dissolved poly(vinyl pyrrolidone) (0.188 g; type K-30). The solution was deoxygenated and subsequently polymerized (24 h; 70 °C). Resulting particles were washed three times with ethanol. The particles were stained using a soaking procedure.[25] PS particles (300 mg), distilled water (20 mL), and THF (15 mL) were mixed and sonicated (30 min) to swell the microbeads. Simultaneously, a solution of platinum 5,10,15,20-tetrakis-(2,3,4,5,6-pentafluorophenyl)porphyrin (Pt-TPFPP) in THF (5 mL; 1.0 mg mL^{-1}) was added dropwise (0.2 mL s^{-1}). Further sonification (20 min) ensured that virtually all dye molecules were inside the hydrophobic PS particles. The THF was evaporated using rotary evaporation.

The general procedure for the conjugation of fluorescein isothiocyanate (FITC) to aminocellulose (AC) follows an earlier method.[5] The AC particles (500 mg; from Presens GmbH; www.presens.de) were prepared by reacting them with FITC (15 mg) in sodium bicarbonate buffer (18 mL, 50 mM, pH 9) for 2 h. Residual amino groups on the particles were blocked by reacting them (100 mg) with acetic anhydride (200 mg) in ethanol (95% v/v, 10 mL) for 12 h at room temperature.

The DPA-PAN reference particles were synthesized by incorporating diphenylanthracene (DPA) in poylacrylonitrile (PAN) using a precipitation method.[26] The particles precipitate from a solution of DPA (30 mg) and PAN (300 mg) in dimethylformamide (30 mL) upon slow addition (1 mL s^{-1}) of distilled water (70 mL) and subsequent addition of brine (20 mL). They can be separated by centrifugation.

All sensor particles were washed four times with ethanol and four times using distilled water (each washing step followed by centrifugation for 10 min at 1030 g). Particles were freeze-dried before storage. Particle sizes were determined by transmission electron microscopy.

Preparation of the sensor films: Pt-PS (50 mg), FITC-AC (70 mg), and DPA-PAN (20 mg) were mixed with an ethanol/water (4 mL; 9:1 v/v) solution containing 5% w/v of the polyurethane hydrogel (type D4; from Cardiotech) to form a sensor "cocktail".[27] The sensor films were then prepared by knife-coating the cocktail on a polyester support by analogy to a method described previously.[5] Particle distribution inside the sensor foils was investigated using fluorescence microscopy prior to use. A representative sample in is shown in Figure 2 d.

The RGB imaging setup (Supporting Information, Figure S2) consists of a standard digital camera (Canon EOS 50D), a modified ring light with 28 LEDs (405 nm peak wavelength; UV5TZ-405-15 BIVAR), and a GG435 emission filter (Schott). Camera parameters were set as follows: Raw + jpg; ISO 160; white balance 2450 K. Excessive ambient light is to be avoided. The image data were stored as 16-bit TIFs using the Adobe Camera Raw plug-in for Adobe Photoshop and data were further processed with ImageJ software using a self-programmed macro file (Supporting Information, macro file M1).[10,28]

Received: June 30, 2011
Published online: September 27, 2011

Keywords: diagnostics · dual sensing · fluorescence · imaging · wound healing

[1] G. Liebsch, I. Klimant, B. Frank, G. Holst, O. S. Wolfbeis, *Appl. Spectrosc.* **2000**, *54*, 548.
[2] P. Niethammer, C. Grabher, A. T. Look, T. J. Mitchison, *Nature* **2009**, *459*, 996.
[3] a) G. Zhang, G. M. Palmer, M. W. Dewhirst, C. L. Fraser, *Nat. Mater.* **2009**, *8*, 747; b) S. Sakadžić, E. Roussakis, M. A. Yaseen, E. T. Mandeville, V. J. Srinivasan, K. Arai, S. Ruvinskaya, A. Devor, E. H. Lo, S. A. Vinogradov, D. A. Boas, *Nat. Methods* **2010**, *7*, 755.
[4] B. F. Grewe, D. Langer, H. Kasper, B. M. Kampa, F. Helmchen, *Nat. Methods* **2010**, *7*, 399.
[5] S. Schreml, R. J. Meier, O. S. Wolfbeis, M. Landthaler, R.-M. Szeimies, P. Babilas, *Proc. Natl. Acad. Sci. USA* **2011**, *108*, 2432.
[6] M. I. J. Stich, L. H. Fischer, O. S. Wolfbeis, *Chem. Soc. Rev.* **2010**, *39*, 3102.
[7] a) D. F. Wilson, G. J. Cerniglia, *Cancer Res.* **1992**, *52*, 3988; b) W. L. Rumsey, J. M. Vanderkooi, D. F. Wilson, *Science* **1988**, *241*, 1649.
[8] S. Schreml, R. J. Meier, O. S. Wolfbeis, T. Maisch, R.-M. Szeimies, M. Landthaler, J. Regensburger, F. Santarelli, I. Klimant, P. Babilas, *Exp. Dermatol.* **2011**, *20*, 550.
[9] S. Bassnett, L. Reinisch, D. C. Beebe, *Am. J. Physiol.* **1990**, *258*, C171.
[10] X. D. Wang, R. J. Meier, M. Link, O. S. Wolfbeis, *Angew. Chem.* **2010**, *122*, 5027; *Angew. Chem. Int. Ed.* **2010**, *49*, 4907.
[11] a) S. Schreml, R. M. Szeimies, S. Karrer, J. Heinlin, M. Landthaler, P. Babilas, *J. Eur. Acad. Dermatol.* **2010**, *24*, 373; b) S. Schreml, R. M. Szeimies, L. Prantl, S. Karrer, M. Landthaler, P. Babilas, *Br. J. Dermatol.* **2010**, *163*, 257; c) S. Schreml, R. M. Szeimies, L. Prantl, M. Landthaler, P. Babilas, *J. Am. Acad. Dermatol.* **2010**, *63*, 866.
[12] a) C. McDonagh, C. S. Burke, B. D. MacCraith, *Chem. Rev.* **2008**, *108*, 400; b) Y. Amao, *Microchim. Acta* **2003**, *143*, 1; c) X. D. Wang, H. X. Chen, Y. Zhao, X. Chen, X. R. Wang, *TrAC Trends Anal. Chem.* **2010**, *29*, 319.
[13] M. I. J. Stich, S. M. Borisov, U. Henne, M. Schaeferling, *Sens. Actuators B* **2009**, *139*, 204.
[14] D. Filippini, A. Alimelli, C. Di Natale, R. Paolesse, A. D'Amico, I. Lundström, *Angew. Chem.* **2006**, *118*, 3884; *Angew. Chem. Int. Ed.* **2006**, *45*, 3800.
[15] B. H. Weigl, A. Holobar, W. Trettnak, I. Klimant, H. Kraus, P. Oleary, O. S. Wolfbeis, *J. Biotechnol.* **1994**, *32*, 127.
[16] L. F. Capitan-Vallvey, A. Lapresta-Fernandez, R. Huertas, M. Melgosa, *Anal. Chim. Acta* **2009**, *636*, 210.
[17] a) L. N. Sun, J. B. Yu, H. S. Peng, J. Z. Zhang, L. Y. Shi, O. S. Wolfbeis, *J. Phys. Chem. C* **2010**, *114*, 12642; b) M. I. J. Stich, S. Nagl, O. S. Wolfbeis, U. Henne, M. Schaeferling, *Adv. Funct. Mater.* **2008**, *18*, 1399.
[18] O. S. Wolfbeis, *Adv. Mater.* **2008**, *20*, 3759.
[19] R. Narayanaswamy, O. S. Wolfbeis, *Optical Sensors for Industrial, Environmental and Clinical Applications*, Springer, Berlin, **2003**, p. 441.
[20] A. Mills, *Chem. Soc. Rev.* **2005**, *34*, 1003.
[21] a) F. S. Ligler, *Anal. Chem.* **2009**, *81*, 519; b) D. R. Walt, Y. N. Kuang, *Biotechnol. Bioeng.* **2007**, *96*, 318; c) M. Kühl, L. F. Rickelt, R. Thar, *Appl. Environ. Microbiol.* **2007**, *73*, 6289.
[22] a) H. Stahl, A. Glud, C. R. Schröder, I. Klimant, A. Tengberg, R. N. Glud, *Limnol. Oceanogr.* **2006**, *4*, 336; b) C. Huber, I. Klimant, C. Krause, T. Werner, T. Mayr, O. S. Wolfbeis, *Fresenius J. Anal. Chem.* **2000**, *368*, 196.
[23] B. Zelelow, G. E. Khalil, G. Phelan, B. Carlson, M. Gouterman, J. B. Callis, L. R. Dalton, *Sens. Actuators B* **2003**, *96*, 304.
[24] Z. L. Zhang, Y. Long, J. B. Pan, X. M. Yan, *J. Mater. Chem.* **2010**, *20*, 1179.
[25] T. Behnke, C. Würth, K. Hoffmann, M. Hübner, U. Panne, U. Resch-Genger, *J. Fluoresc.* **2011**, *21*, 937.
[26] a) J. M. Kürner, I. Klimant, C. Krause, H. Preu, W. Kunz, O. S. Wolfbeis, *Bioconjugate Chem.* **2001**, *12*, 883; b) S. M. Borisov, T. Mayr, G. Mistlberger, K. Waich, K. Koren, P. Chojnacki, I. Klimant, *Talanta* **2009**, *79*, 1322.
[27] S. M. Borisov, A. S. Vasylevska, C. Krause, O. S. Wolfbeis, *Adv. Funct. Mater.* **2006**, *16*, 1536.
[28] M.-S. Steiner, R. J. Meier, A. Duerkop, O. S. Wolfbeis, *Anal. Chem.* **2010**, *82*, 8402.

